nature neuroscience

Dopaminergic neurons promote hippocampal reactivation and spatial memory persistence

Colin G McNamara, Álvaro Tejero-Cantero, Stéphanie Trouche, Natalia Campo-Urriza & David Dupret

We found that optogenetic burst stimulation of hippocampal dopaminergic fibers from midbrain neurons in mice exploring novel environments enhanced the reactivation of pyramidal cell assemblies during subsequent sleep/rest. When applied during spatial learning of new goal locations, dopaminergic photostimulation improved the later recall of neural representations of space and stabilized memory performance. These findings reveal that midbrain dopaminergic neurons promote hippocampal network dynamics associated with memory persistence.

Brain representations of space are encoded by pyramidal cell assemblies in the hippocampus during active behavior[1–3]. However new representations, such as those formed during exploration of novel environments or learning of new goal locations, are initially labile and therefore require stabilization to persist as memories[4–6]. Pharmacological studies have implicated the neurotransmitter dopamine in the stability of hippocampus-dependent memory. Blockade of D1/D5 dopaminergic receptors during spatial learning impairs memory persistence[7], whereas blockade during exploration of novel environments curtails the stability of new spatial maps[8] and prevents novelty-facilitated synaptic plasticity[9]. However the contribution of dopamine to hippocampal neuronal dynamics associated with memory persistence remains to be identified[10]. In the hippocampus, memory stabilization is thought to be supported by 'sleep reactivation', whereby assembly firing patterns expressed during exploration are reactivated in subsequent sleep/rest periods during sharp wave/ripple (SWR, 135–250 Hz) oscillatory events[11,12]. Indeed, electrical disruption of SWRs after learning impairs spatial memory[13]. We tested whether activation of midbrain dopaminergic neurons during spatial exploration and learning enhances reactivation of newly encoded hippocampal representations and improves memory performance.

To identify and control the activity of midbrain neurons expressing the dopamine transporter (DAT), we injected a Cre-inducible viral construct encoding Channelrhodopsin-2 fused to enhanced yellow fluorescent protein (ChR2-eYFP)[14] into the ventral tegmental area (VTA) of *DAT-IRES-Cre*$^{+/-}$ mice (**Fig. 1a**). In these DAT^{VTA}::ChR2-eYFP mice, 98.6 ± 0.4% of ChR2-expressing VTA neurons coexpressed tyrosine hydroxylase (TH), demonstrating a highly specific targeting of dopaminergic neurons, with 76 ± 7% of TH-immunopositive neurons coexpressing ChR2-eYFP (n = 4 mice; **Fig. 1b**). In addition to their presence in other brain areas, such as the striatum, axons coexpressing ChR2-eYFP and TH were found extending along the antero-posterior axis of the CA1 region of dorsal hippocampus (dCA1) with collaterals in the strata radiatum, pyramidale and oriens (**Fig. 1c**,**d**). Consistent with earlier reports, these data highlight the structural substrate by which midbrain-derived dopamine could modulate hippocampal dynamics[10,15].

To determine whether the activity of dopaminergic neurons affects dCA1 pyramidal cell assemblies, we combined *in vivo* multichannel recordings with photostimulation in eight DAT^{VTA}::ChR2-eYFP mice and two DAT^{VTA}::eYFP control mice exploring novel open field environments (n = 1,363 dCA1 pyramidal neurons yielding 25,510 cell pairs; **Supplementary Table 1**). Photostimulation was targeted at either dopaminergic neurons in the VTA (VTA-ON configuration) or directly at their axons in dCA1 (dCA1-ON; **Fig. 1a**). Mice also explored familiar and novel environments without photostimulation to provide a baseline to assess changes in network activity. In these non-photostimulated sessions, we found that the firing rate of VTA neurons (n = 157) increased in novel environments compared with the familiar ones (novelty-induced rate change = 0.56 ± 0.14 Hz, t_{156} = 3.88, P = 0.00016, paired t test; **Fig. 1e**,**f** and **Supplementary Fig. 1**). This VTA firing response to spatial novelty, which might be partially informed by hippocampal spatio-contextual inputs[10,16], resulted in a higher fraction of action potentials discharged in bursts (interspike interval < 50 ms; novelty-induced burst ratio change = 0.31 ± 0.07, t_{156} = 4.31, $P = 2.9 \times 10^{-5}$, paired t test), a potentially suitable signal to in turn modulate hippocampal dynamics. In addition, we confirmed that firing associations between dCA1 pyramidal cells reorganized to represent each environment[2,4,5,17] (**Supplementary Fig. 2a**).

To measure SWR reactivation, we recorded sleep/immobility rest sessions after each exploration. We found that VTA-ON and dCA1-ON burst-mode photostimulation (**Fig. 2a**) during exploration of novel environments enhanced the subsequent reactivation of hippocampal waking firing patterns (**Fig. 2b**) without altering exploratory behavior or the arousal state in rest (**Supplementary Figs. 3a–c** and **4**). Reactivation was measured by comparing the tendency of pyramidal cell pairs to co-fire in cycles of theta oscillations (5–12 Hz) during active exploration (theta co-firing; **Supplementary Fig. 3d–g**) with their tendency to co-fire in SWR events during following rest (SWR co-firing)[6,17]. For all conditions, reactivation strength (the correlation of the waking theta co-firing patterns with subsequent rest SWR co-firing patterns) was higher than in a baseline comparison with SWR patterns from the initial rest before all exploration (all P < 0.0001; **Fig. 2b** and **Supplementary Table 2**). Moreover, hippocampal patterns representing novel environments were more strongly reactivated in post-exploration SWRs than the old, well-established ones mapping the familiar environment (z = 4.79, $P = 1.7 \times 10^{-6}$; **Fig. 2b** and **Supplementary Table 3**). This is consistent with the hypothesis that SWR reactivation supports the consolidation of newly formed neuronal assemblies[17]. Notably, we found that burst-mode

Medical Research Council Anatomical Neuropharmacology Unit, Department of Pharmacology, University of Oxford, Oxford, UK. Correspondence should be addressed to D.D. (david.dupret@pharm.ox.ac.uk) or C.G.M. (colin.mcnamara@pharm.ox.ac.uk).

Received 28 July; accepted 23 September; published online 19 October 2014; doi:10.1038/nn.3843

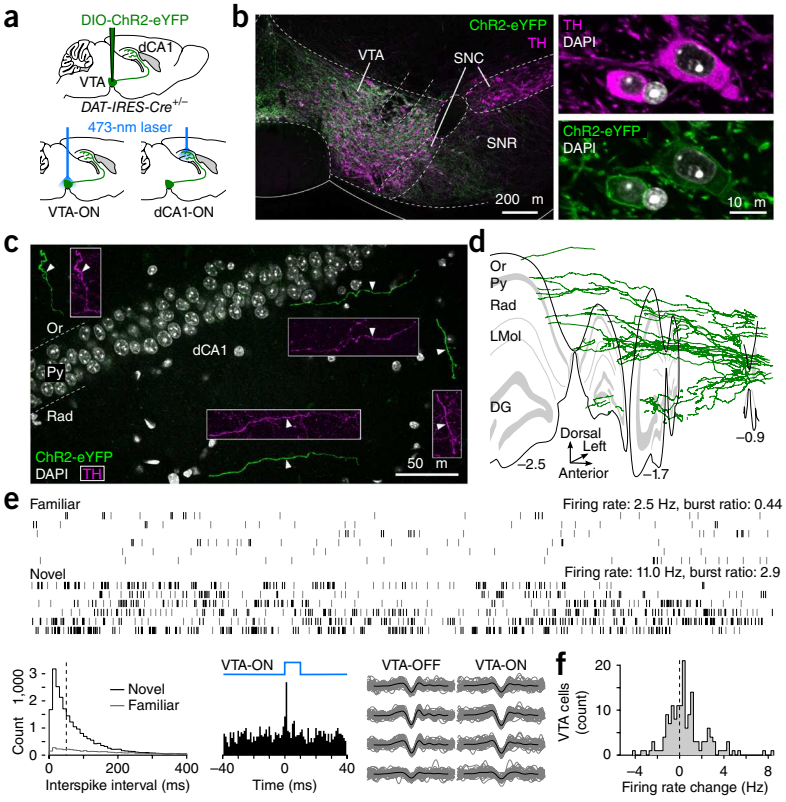

Figure 1 Midbrain dopaminergic neurons increase their discharge in novel environments. (**a**) Virus injection and photostimulation configurations. (**b**) ChR2-eYFP expression targeting VTA dopaminergic neurons as identified by TH immunoreactivity. Cell nuclei were stained using DAPI. (**c**) ChR2-expressing dopaminergic axons in dCA1. Insets show corresponding TH immunoreactivity (flattened 70-µm *z* stack; DAPI, 1-µm confocal plane). (**d**) Three-dimensional reconstruction of ChR2-expressing axons in the dorsal hippocampus (distances from bregma in mm). (**e**) Spike times (top) of an optogenetically identified dopaminergic neuron in familiar and novel environments (1-min raster plot, 10-s rows, ticks represent spikes, bursts shown in black; **Supplementary Fig. 1**) with interspike interval distributions (left), laser-triggered firing probability histogram (middle) and spontaneous (VTA-OFF) versus light-evoked (VTA-ON) spike waveforms (right); photostimulation subsequent to shown explorations, mean waveforms superimposed in black. (**f**) Distribution of firing rate change in response to spatial novelty for VTA neurons having a mean rate between 1 and 12 Hz. DG, dentate gyrus; LMol, stratum lacunosum-moleculare; Or, stratum oriens; Py, stratum pyramidale; Rad, stratum radiatum; SNC, substantia nigra pars compacta; SNR, substantia nigra pars reticulata.

photoactivation of dopaminergic neurons enhanced hippocampal reactivation further (VTA-ON: $z = 2.53$, $P = 0.011$; dCA1-ON: $z = 6.52$, $P = 7.2 \times 10^{-11}$; **Fig. 2b**) without altering the mean firing rate, spatial tuning or cross-environment reorganization of pyramidal assemblies (**Supplementary Fig. 2**). Neither the mean firing rate nor the proportion of spiking pyramidal cells during SWRs were changed (**Supplementary Fig. 5**). Enhanced reactivation therefore represents an increased similarity of the SWRs assembly patterns to the previous waking ones. Such enhanced reactivation was blocked by the D1/D5 antagonist SCH23390 when it was injected before exploration and was not observed in control mice transfected with a construct coding for eYFP only (**Fig. 2b** and **Supplementary Table 3**). Furthermore, tonic-mode stimulation consisting of the same number of light pulses (now equally spaced) produced only a weak trend of increased reactivation ($z = 1.94$, $P = 0.052$; **Fig. 2b**). Collectively these data demonstrate that burst-mode activation of dopaminergic neurons increases hippocampal reactivation in a D1/D5 receptor–dependent manner.

We next tested whether dopamine-enhanced reactivation was associated with the strengthening of new spatial memories, as expressed by the reinstatement of newly learned representations alongside stable behavioral performance. We performed bilateral dCA1-ON burst-mode photostimulation with dCA1 recording in four DAT^{VTA}::ChR2-eYFP mice (560 dCA1 pyramidal cells yielding 12,072 cell pairs; **Supplementary Table 1**) trained to a hippocampus-dependent learning task on a crossword-like maze (**Fig. 3a** and **Supplementary Fig. 6**). On each day, mice first explored the maze without barriers (pre-learning) to provide a baseline to assess learning-related changes in network activity. Then, for the 'learning' stage, two start boxes were selected and a food reward was introduced together with a new arrangement of barriers so that only one path from each start box led to the reward location. Mice had 20 trials to learn the new configuration and find the reward.

Behavioral performance gradually improved with learning trials, as measured by a shortening of distance traveled from start box to reward in each trial (**Fig. 3a**,**b**). Notably, photostimulation during learning prevented the degradation of memory performance in a probe test held 1 h later ($t_{23} = 4.99$, $P = 4.8 \times 10^{-5}$, *t* test; **Fig. 3b**), despite not affecting learning performance ($F_{19, 405} = 0.40$, $P = 0.99$, ANOVA; **Fig. 3b**). The reorganization of hippocampal spatial maps between the pre-learning and the learning periods was also unaffected by photostimulation (**Fig. 3c**,**d** and **Supplementary Fig. 7**). However, the reinstatement of the newly learned spatial maps in the probe test was promoted following activation of dCA1 dopaminergic axons ($z = 5.90$, $P = 3.6 \times 10^{-9}$; **Fig. 3d**), a phenomenon associated with memory recall[6]. The persistence of memories was associated with the strength of hippocampal reactivation. Hippocampal firing patterns expressed during learning were more strongly reactivated in

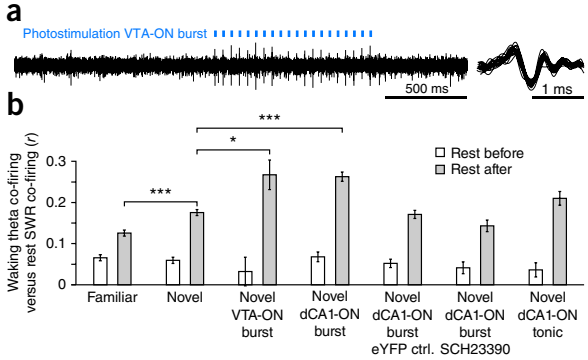

Figure 2 Burst-mode photostimulation of dopaminergic neurons during exploration enhances reactivation of new hippocampal assemblies. (**a**) High pass–filtered VTA single-channel tetrode recording (left) showing firing response to burst-mode photostimulation (trains of 20 10-ms pulses at 50-ms intervals) and superimposed waveforms of all 20 light-driven spikes (right). (**b**) SWR reactivation of dCA1 co-firing patterns (**Supplementary Tables 2** and **3**). *r* represents Pearson correlation coefficient. Error bars represent s.e. $*P < 0.05$, $***P < 0.001$.

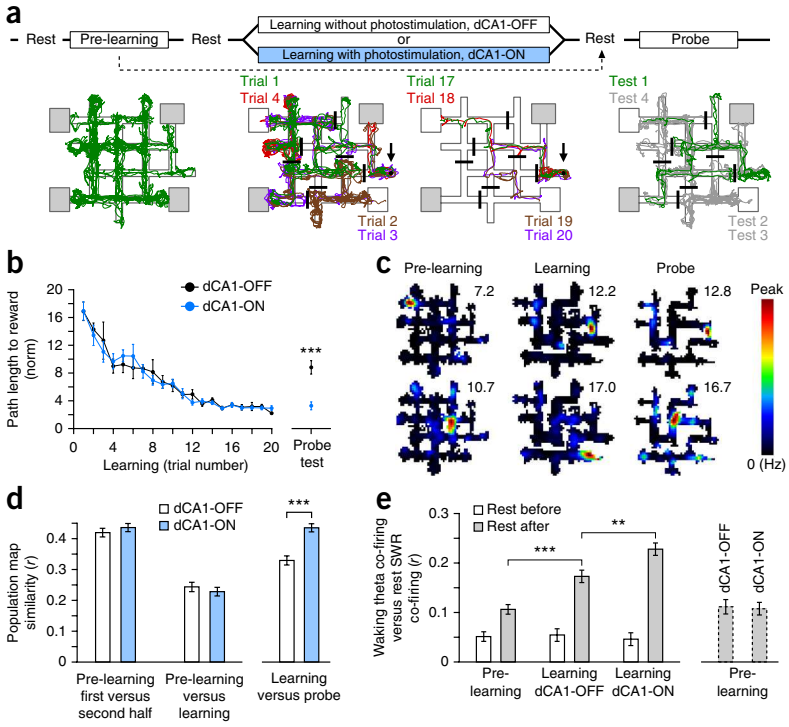

Figure 3 Burst-mode photostimulation of dCA1 dopaminergic axons during spatial learning on the crossword maze stabilizes new hippocampal maps and memory of new goal locations. (**a**) Protocol with example single-day single-animal trajectories. Solid arrows indicate the reward location for that day; in-use start boxes are shown in white. (**b**) Photostimulation did not alter path shortening to reward during learning (left), but did stabilize performance in the probe (right; $P = 4.8 \times 10^{-5}$, *t* test, dCA1-ON versus dCA1-OFF). Error bars represent s.e.m. (**c**) Example rate maps for two dCA1 cells (one per row) establishing a new firing field in learning that was reinstated for the top cell only during the probe (**Supplementary Fig. 7**). Numbers indicate peak firing rate. (**d**) Photostimulation did not affect spatial map reorganization between pre-learning and learning (left), but did promote reinstatement of newly established maps during the probe (right; $P = 3.6 \times 10^{-9}$). *r* represents Pearson correlation coefficient. Error bars represent s.e. (**e**) SWR-reactivation after learning was higher than after pre-learning and increased further following photostimulation (left; **Supplementary Tables 2** and **3**). However, photostimulation did not extend its effect to the previously expressed assemblies (right; see dashed arrow in **a**). *r* represents Pearson correlation coefficient. Error bars represent s.e. $^{**}P < 0.01$, $^{***}P < 0.001$.

subsequent rest than the pre-learning patterns were in the rest after pre-learning exploration ($z = 4.23$, $P = 2.3 \times 10^{-5}$; **Fig. 3e**). Photostimulation during learning further enhanced the reactivation of the concurrently expressed firing patterns ($z = 3.16$, $P = 0.0016$; **Fig. 3e**), but did not extend its effect back to the patterns expressed during the pre-learning exploration ($z = 0.21$, $P = 0.84$; **Fig. 3e**). This finding indicates that dopamine acts specifically on actively expressed neuronal assemblies.

Determining the network-level processes underpinning the specific stabilization of some newly acquired engrams (while others fade) is critical for a comprehensive understanding of memory. Our findings demonstrate that dopaminergic activity at the time of formation of new hippocampal cell assemblies increases the subsequent off-line SWR reactivation of these assemblies. Such reactivation is thought to enable the incorporation of new memory engrams, especially those associated with novel and rewarded outcomes, into stable representations capable of informing future behavior[6,11,12,18]. Accordingly, we found that dopaminergic-enhanced reactivation prevents the degradation of learned behavioral performance while concurrently strengthening the reinstatement of the newly acquired spatial representation. Thus, our results provide insights into the relationship between midbrain dopaminergic neurons, encoding salient information about an environment[9,10,16,19,20], and hippocampal assemblies, providing representations of space[1–3], in modulating memory according to the value of the information to be remembered.

METHODS

Methods and any associated references are available in the online version of the paper.

Note: Any Supplementary Information and Source Data files are available in the online version of the paper.

ACKNOWLEDGMENTS

We thank J. Csicsvari, P. Somogyi and P.J. Magill for their comments on a previous version of the manuscript, C. Etienne for her assistance with axon reconstruction, S. Cuell for his initial contribution with the crossword maze, S. Threfell and L. Norman for their assistance with the *DAT-IRES-Cre* mice, and K. Deisseroth (Stanford University) for sharing the DIO-ChR2-eYFP and DIO-eYFP constructs. C.G.M. is funded by a Medical Research Council Doctoral Training Award. This work was supported by the Medical Research Council UK (award MC_UU_12020/7) and a Mid-Career Researchers Equipment Grant from the Medical Research Foundation (award C0443) to D.D.

AUTHOR CONTRIBUTIONS

C.G.M., Á.T.-C. and D.D. designed the experiments. C.G.M., N.C.-U. and S.T. carried out the experiments. C.G.M. and D.D. analyzed the data and wrote the manuscript. Á.T.-C. and S.T. edited the manuscript. D.D. conceived and supervised the project. All of the authors discussed the results and commented on the manuscript.

COMPETING FINANCIAL INTERESTS

The authors declare no competing financial interests.

1. O'Keefe, J. *Exp. Neurol.* **51**, 78–109 (1976).
2. Wilson, M.A. & McNaughton, B.L. *Science* **261**, 1055–1058 (1993).
3. Moser, E.I., Kropff, E. & Moser, M.B. *Annu. Rev. Neurosci.* **31**, 69–89 (2008).
4. Kentros, C. *et al. Science* **280**, 2121–2126 (1998).
5. Frank, L.M., Stanley, G.B. & Brown, E.N. *J. Neurosci.* **24**, 7681–7689 (2004).
6. Dupret, D., O'Neill, J., Pleydell-Bouverie, B. & Csicsvari, J. *Nat. Neurosci.* **13**, 995–1002 (2010).
7. Bethus, I., Tse, D. & Morris, R.G.M. *J. Neurosci.* **30**, 1610–1618 (2010).
8. Kentros, C.G., Agnihotri, N.T., Streater, S., Hawkins, R.D. & Kandel, E.R. *Neuron* **42**, 283–295 (2004).
9. Li, S., Cullen, W.K., Anwyl, R. & Rowan, M.J. *Nat. Neurosci.* **6**, 526–531 (2003).
10. Lisman, J.E. & Grace, A.A. *Neuron* **46**, 703–713 (2005).
11. Buzsáki, G. *Neuroscience* **31**, 551–570 (1989).
12. Wilson, M.A. & McNaughton, B. *Science* **265**, 676–679 (1994).
13. Girardeau, G., Benchenane, K., Wiener, S.I., Buzsáki, G. & Zugaro, M.B. *Nat. Neurosci.* **12**, 1222–1223 (2009).
14. Tsai, H.-C. *et al. Science* **324**, 1080–1084 (2009).
15. Scatton, B., Simon, H., Le Moal, M. & Bischoff, S. *Neurosci. Lett.* **18**, 125–131 (1980).
16. Luo, A.H., Tahsili-Fahadan, P., Wise, R.A., Lupica, C.R. & Aston-Jones, G. *Science* **333**, 353–357 (2011).
17. O'Neill, J., Senior, T.J., Allen, K., Huxter, J.R. & Csicsvari, J. *Nat. Neurosci.* **11**, 209–215 (2008).
18. Singer, A.C. & Frank, L.M. *Neuron* **64**, 910–921 (2009).
19. Cohen, J.Y., Haesler, S., Vong, L., Lowell, B.B. & Uchida, N. *Nature* **482**, 85–88 (2012).
20. Schultz, W., Dayan, P. & Montague, P.R. *Science* **275**, 1593–1599 (1997).

ONLINE METHODS

Approval for experiments with animals. Experiments involving animals were conducted according to the UK Animals (Scientific Procedures) Act 1986 under personal and project licenses issued by the Home Office following ethical review.

Subjects and surgical procedures. All *DAT-IRES-Cre*$^{+/-}$ animals used (**Supplementary Table 1**) were male adult transgenic heterozygote mice (3–8 months old) and bred from homozygotes for DAT-internal ribosome entry site (IRES)-Cre (Jackson Laboratories, B6.SJL-Slc6a3$^{tm1.1(cre)Bkmn}$/J, stock number 006660)[21]. Animals were housed with their littermates until used in the procedure with free access to food and water in a dedicated housing room with a 12/12-h light/dark cycle. Surgical procedures were performed under deep anesthesia using isoflurane (0.5–2%) and oxygen (2 l min^{-1}). Analgesia was also provided (buprenorphine, 0.1 mg per kg of body weight). To generate expression of ChR2 in dopamine neurons, we used a Cre-*loxP* approach by injecting a Cre-inducible recombinant viral vector containing ChR2-eYFP (pAAV$_2$-EF1a-DIO-hChR2(H134R)-eYFP-WPRE, 2.5 × 10^{12} molecules per µl, Virus Vector Core) in DAT-IRES-Cre mice at a rate of less than 0.1 µl min^{-1} using a glass micropipette as described previously[22]. Two additional *DAT-IRES-Cre*$^{+/-}$ animals were injected with a control viral vector coding for the eYFP only (pAAV$_2$-EF1a-DIO-eYFP, 2.5 × 10^{12} molecules per µl, Virus Vector Core). Viral vector injections (1 µl each) were performed to the right hemisphere or bilaterally. All crossword maze animals received a bilateral injection and implant. Each injection was delivered to the VTA using stereotaxic coordinates 3.25 mm posterior, ±0.5 mm lateral from bregma and 3.8–4 mm ventral from the brain surface. 4 weeks were allowed for virus expression before recording commenced. To test for the hippocampus dependency of the crossword maze task, *PV-IRES-Cre*$^{+/+}$ adult male mice (n = 5; Jackson Laboratories, B6;129P2-Pvalb$^{tm1(cre)Arbr}$/J, stock number 008069) were used with the same approach, but to transfect PV-expressing interneurons bilaterally in the dCA1 region with the ChR2-eYFP viral vector using stereotaxic coordinates 2.00 mm posterior, ±1.6 mm lateral from bregma and 1.2 mm ventral from the brain surface for injection. Implanted mice received eight or ten independently movable tetrodes, constructed as described previously[6,17], and one or two optic fibers (Doric lenses, Québec, Canada). To enable their independent movement, each tetrode was attached to a M1.4 screw and all tetrodes were assembled in a microdrive containing the optic fibers before implantation. This also ensured that the optic fiber was completely enclosed to prevent escaped light illuminating the environment. Optic fibers targeted at dCA1 were positioned 2 mm posterior and 1.6 mm lateral from bregma and lowered into the brain a distance of 0.9–1 mm. Tetrodes were typically located within 0.5 mm of the optic fiber. For simultaneous midbrain and hippocampal recordings with VTA targeted optic fiber the implant was positioned at a 40 degree angle from the antero-posterior axis on the horizontal plane and then at an angle of 10 degrees from the dorso-ventral axis. The optic fiber was positioned at 2.7 mm posterior and 1 mm lateral from bregma and lowered into the brain at the angle described a distance of 3.9–4.2 mm. All tetrodes were initially implanted slightly above the recording location of interest.

Data acquisition and photostimulation. Each signal was buffered on the head of the animal using an operational amplifier in a non-inverting unity gain configuration (Axona) and transmitted over a single strand of litz wire to a dual stage amplifier and band pass filter (gain 1000, pass band 0.1 Hz to 5 kHz, Sensorium). The amplified and filtered signals along with a synchronization signal from the position tracking system and the activation signal for the laser were digitized at a rate of 20 kHz and saved to disk by a PC with 16 bit analog to digital converter cards (United Electronics Industries). To track the location of the animal three LED clusters (red, green and blue) were attached to the electrode casing above the head of the animal and captured at 25 frames per s by an overhead color camera (Sony). The camera was attached to a PC that extracted the position data in real time. Photostimulation was generated using a 473-nm diode-pumped solid-state laser (Laser 2000, Ringstead) and delivered to the brain through two lengths of optic fiber (with black plastic jackets to prevent illumination of the environment) and a rotary joint with splitter in the case of bilaterally implanted animals (Doric Lenses). The final optic fibers (on the animal end) were coupled to the implanted fiber using an M3 connector. The output intensity delivered to the implanted fiber was approximately 20 mW. Open field DAT-IRES-Cre mice received either burst-mode photostimulation (trains of 20 light pulses 10 ms in duration with pulses at 50-ms intervals and a burst train delivered every 40 s) or tonic-mode photostimulation (single light pulses 10 ms in duration delivered every 2 s). For the crossword maze experiments additional DAT-IRES-Cre mice received burst-mode photostimulation with pulse duration of 20 ms and burst trains delivered every 20 s. For experiments aimed at disrupting hippocampal network activity by local stimulation of PV-expressing interneurons, PV-IRES-Cre mice received 473-nm photostimulation applied randomly to 80% of the learning trials using trains of 10-ms pulses every 16 ms. The laser was off during the inter-trial intervals. In all of these experiments, each mouse alternated between days with photostimulation OFF and days with photostimulation ON.

Post-recovery and recording. After initial recovery from implantation, and before recording commenced, each mouse was connected to the recording apparatus and familiarized (through spontaneous exploration) with the familiar open field environment or crossword maze (without barriers) as applicable. This typically lasted 1–2 h a day for at least a week. During this time, tetrodes were gradually lowered over days through the short distance remaining to reach the required brain area. All recorded mice were also familiarized with a 12- × 12-cm high-walled box containing home cage bedding which was used for rest recordings (sleep and long periods of awake immobility).

At the start of each recording day hippocampal tetrodes were lowered into stratum pyramidale and midbrain ones were moved slightly in search of action potentials. The animal was then left in the home cage for at least 1 h before recording started. All recordings were performed during day time and the random assignment of each subject to the various experimental conditions is reported in **Supplementary Table 1**. At the end of each recording day, hippocampal tetrodes were raised slightly to minimize mechanical damage caused to the stratum pyramidale by tetrodes left in this layer overnight and to maximize the cell yield and number of recording days per mouse. No further recording days were performed once the number of cells decreased below the number of cells obtained in the initial days. Stratum pyramidale was located using the profile of SWR events and presence of multiunit spiking activity. Recordings were always performed in the same room under dim lighting with the recording arena surrounded by a black circular curtain. Rest recordings were approximately 30 min in duration. Investigators were aware as to which experimental conditions each subject had to be exposed to (for example, familiar versus novel, photostimulation OFF versus ON, exploration versus sleep). Open field recording arenas consisted of various boxes of different shapes (polygons with some curved edges surrounded by walls, approximate area generally near 0.25 m^2) constructed from plastic or wood (sometimes lined with brown paper). Open field exploration recording sessions were approximately 30 min in duration. To determine whether enhanced SWR reactivation following burst-mode photostimulation of dopaminergic terminals in dCA1 required activation of dopaminergic receptors, mice were injected with SCH23390, a selective and potent antagonist of D1/D5 dopaminergic receptors (Sigma, #D054, 0.1 mg per kg in 0.9% saline (wt/vol), intraperitoneal) 30 min before the exploration of a novel environment.

Crossword maze. The crossword-like maze (**Fig. 3a** and **Supplementary Fig. 6a**) consisted of four start boxes and eight intersecting open tracks forming 14 intersections inspired by a layout used previously[23]. The width of each track was 5 cm with a 1.5-cm-high rim along the edges. The entire maze measured 95 × 95 cm excluding start boxes. The maze was painted black and suspended 5 cm above a black table. Distal cue cards were placed on the curtain surrounding the maze and some cue objects were placed on the supporting table dispersed throughout the maze. To promote allocentric spatial navigation by distal cues, the maze was randomly rotated relative to the cues at the beginning of each day. Mice performing the crossword maze task were maintained at 85% of their post-operative body weight. The recording protocol used consisted of the following ordered stages: rest, pre-learning, rest, learning, rest and probe (**Fig. 3a**). During the pre-learning stage, the animal explored the maze with the start boxes closed and in the absence of barriers and rewards for approximately 20 min.

For the learning stage two start boxes and one food reward location (at the end of one of the five tracks protruding from the maze) were selected as in use for that day and the maze was configured with a new arrangement of up to seven barriers (10 cm in height) such that there was only one path from each

start box to the reward (**Supplementary Fig. 6a**). Mice were given up to 20 trials (mean = 18.7, median = 19.0, quartile range = 18.0–20.0) to learn to find the reward with the start point randomly switching between the two start boxes. The per trial reward was 4 µl of condensed milk diluted 30% in water and was placed on a plastic cap at the goal location. A similar plastic cap (without reward) was placed in each of the other four tracks protruding from the maze. A glass vial (with perforated lid) containing an aliquot of the reward yet non accessible was placed inside the two start boxes to signal the onset of the learning phase to the animal. The board was cleaned after each learning trial to discourage the use of an odor guided search strategy.

For the probe stage (conducted 1 h after learning), the maze was maintained in the same layout as the learning stage, but no reward was present. Mice were released from one of the in use start boxes and allowed to explore the maze for 3 min. Mice were released a further three times (3 min each, 12-min duration probe in total) during the probe stage in order to ensure good coverage of the maze to calculate spatial rate maps. The path length to first reaching of the reward location was used to evaluate memory performance. When combining across maze configurations, path lengths were normalized by the relevant shortest possible path (**Supplementary Fig. 6a**). The number of crossword maze recording days included in this study is 12 d without photostimulation and 13 d with photostimulation for experiments involving the DAT-IRES-Cre mice; 13 d (12 probe tests) without photostimulation and 9 d with photostimulation for experiments involving the PV-IRES-Cre mice.

Spike detection and unit isolation. The recorded signals were digitally band-pass filtered (800 Hz to 5 kHz) offline for spike detection and unit isolation. Spikes were detected using a threshold in the r.m.s. power (0.2-ms sliding window) of the filtered signal. Unit isolation was performed on the first three or four principal components calculated for each channel recorded by the tetrode in question. This was achieved by automatic overclustering (KlustaKwik, http://klusta-team.github.io/) followed by graphically based manual recombination and further isolation informed by cloud shape in principal component space, cross-channel spike waveforms, auto-correlation histograms and cross-correlation histograms[24,25]. To analyze changes in the firing patterns of pyramidal ensembles over time and reliably monitor cell pairs across recording sessions, we needed to ensure that our sample of cells was taken from clusters with stable firing. We therefore clustered together all of the sessions recorded on a given day. Only well-isolated and stable units over the entire recording day were used for further analysis; namely, units that showed a clear refractory period in their auto-correlations and well-defined cluster boundaries across all recording sessions of the day. Units were deemed independent from each other by their distinct spike waveform, the absence of refractory period in their cross-correlations and separable principal component boundaries using a measure based on the Mahalanobis distance[24,26]. Hippocampal pyramidal cells were identified by their auto-correlogram, firing rate and spike waveform, as previously described[24]. The total number of pyramidal cells included in this study is reported in **Supplementary Table 1**.

Detection of theta oscillations, SWR events and behavioral states. Theta oscillations and SWR events were detected off-line using digital band-pass filter methods as previously described[6,17,24]. First, the theta/delta power ratio was measured in 1,600-ms segments (800-ms steps between measurement windows), using Thomson's multi-taper method[24,27,28]. The theta-delta power ratio was used to mark periods of theta activity and individual theta oscillatory waves were identified within these periods by first applying a conservative band-pass filter (5–28 Hz) to the wideband signal. This allowed precise detection of the trough of individual waves from the filtered trace without over smoothing the signal. Next, phase alignment was performed to these minima and theta windows were demarcated spanning from peak-to-peak. Windows with a corresponding theta frequency of 5–12 Hz were used in further analysis (mean = 7.5 Hz, median = 7.7 Hz, quartile range = 6.7–8.6). These detected theta windows corresponded to periods when the animals were actively exploring the environment (**Supplementary Fig. 3d**). The mean number of theta cycles per waking session used for spike binning was not different across conditions (open field experiments: 5,699.6 ± 165.5, $F_{3,143} = 1.41$, $P = 0.24$, ANOVA; crossword maze experiments = 15,038.5 ± 855.6, $t_{23} = 1.31$, $P = 0.20$, t test; mean ± s.e.m.). SWR event detection was performed in rest epochs when the instantaneous speed of the animal was less than 2 cm s^{-1} and the theta-delta ratio was less than 2. Recorded signals were band-pass filtered (135–250 Hz), and the signal from a ripple-free reference electrode was subtracted to eliminate common-mode noise (such as muscle artifacts). Next the power (root mean square) of the processed signal was calculated for each electrode and summed across CA1 pyramidal cell layer electrodes to reduce variability. The threshold for SWR event detection was set to 7 s.d. above the background mean power. The proportion of pyramidal cells active in SWR events was calculated for recordings with at least five pyramidal cells. The SWR firing rate histograms of pyramidal cells were calculated using 20-ms bins in reference to the SWR peak (that is, peak of ripple-band power).

Novelty-related change in VTA firing activity. Firing response of VTA neurons to spatial novelty was assessed by the change in firing rate and burst ratio during exploration of familiar versus novel environments in the absence of photostimulation. The burst ratio measure was calculated as the total number of burst spikes divided by the total number of single spikes. This allowed longer bursts with many spikes to have a more representative contribution to the ratio than spike doublets or triplets compared to measures that count all bursts equally irrespective of length. Bursts were classified as trains of at least two spikes with interspike intervals of less than 50 ms. This conservative intraburst spike interval threshold of 50 ms (intraburst frequency of 20 Hz) was chosen over the often used 80-ms (12.5 Hz) start with greater than 160-ms (6.25Hz) end of a burst criteria established in anesthetized rats[29,30] to allow sufficient clearance between the burst interval threshold frequency and some of the higher mean rates (11 Hz) seen in our light-identified units from behaving mice. Note that use of a 80-ms cut-off produced similar findings. The 160-ms end of burst criteria was also not needed as it was originally included to allow for the observation that there is often a missed spike in a burst that isolates the later spikes from the first spikes of the same burst[29], but the burst ratio measure used here takes into account all burst spikes. These measures were generated from the first 10 min of each exploration to capture best the times of maximal novel experience. Cells included in this analysis had a mean firing rate of between 1 and 12 Hz in both the familiar and novel environments calculated separately. These rate boundaries were chosen to match that reported for VTA dopaminergic neurons in behaving mice[19] and the mean rates of the light-driven units we identified in separate VTA-ON recording sessions on the same days.

Reactivation. Reactivation strength was measured as the Pearson correlation coefficient between the tendencies of hippocampal pyramidal cell pairs to fire together (co-fire) across theta cycles during exploration (theta co-firing) with their tendency to co-fire in SWR events during rest (SWR co-firing)[6,17]. To measure theta co-firing during exploration, we first established for each pyramidal cell its instantaneous firing rate counts (IFRC) in windows spanning from peak-to-peak of detected theta cycles and then we calculated the correlation coefficient between the IFRCs for each cell pair. Likewise, SWR co-firing values were calculated as the correlation coefficients between IFRCs of pyramidal cell pairs taken from 100-ms windows centered on the peak power of SWR events. The reactivation strength was then calculated as the Pearson correlation coefficient between the theta bin co-firing values and the SWR bin co-firing values. Detected theta windows corresponded to periods of active exploration and SWR events were restricted to times of behavioral immobility. Only simultaneously recorded cells were paired. The total number of pyramidal cell pairs for each condition is reported in **Supplementary Table 1**.

Spatial rate maps. The horizontal plane of the recording arena was divided into bins of approximately 2 × 2 cm to generate spike count maps (number of spikes fired in each bin) for each unit and an occupancy map (time spent by the animal in each bin). All maps were then smoothed by convolution with a Gaussian kernel having s.d. equal to one bin width. Finally, spatial rate maps were generated by normalizing (dividing) the smoothed spike count maps by the smoothed occupancy map.

Population map similarity. The population map similarity measure as applied previously[6,17] compares all the place maps from two different time periods in a pairwise fashion in the same manner as the co-firing analysis does for cell firing patterns across LFP events by performing binning over space rather than time. It represents the degree to which cells which fired in similar regions of space (that is, overlapping place fields) still fire in similar regions of space later. It is calculated

doi:10.1038/nn.3843

by first computing the place field similarity (PFS) value for each cell pair during the first time period as the Pearson correlation coefficient from the direct bin wise comparisons between the spatial rate maps of the two cells limited to valid bins (occupancy greater than zero). This is repeated for the second time period and the population map similarity between the two time periods is then calculated as the Pearson correlation coefficient between the PFS values from each of the time periods. Hippocampal place cells screened for their spatial tuning using a sparsity value of no more than 0.3 were included in this analysis[6]. Note that, in the case of assessing map reinstatement during the memory probe test, the PFS values calculated from the second half of the learning trials were compared to PFS values from the probe tests.

Spatial tuning measures. Coherence and sparsity were calculated from the unsmoothed place rate maps as reported before[31,32]. Coherence reflects the similarity of the firing rate in adjacent bins, and is the z transform of the Pearson correlation (across all bins) between the rate in a bin and the average rate of its eight nearest neighbors[31]. Sparsity corresponds with the proportion of the environment in which a cell fires, corrected for dwell time, and is defined as $(\Sigma P_i R_i)^2/\Sigma P_i R_i^2$, where P_i is the probability of the mouse occupying bin i and R_i is the firing rate in bin i (ref. 32).

Error intervals and statistical tests. All error intervals quoted are ±s.e.m. or s.e. of the correlation coefficient calculated as the square root of $(1 - r^2)/(n - 2)$, where r is the Pearson correlation coefficient and n is the number of cell pairs[33]. All tests performed were two sided. All P values for the comparison of Pearson correlation coefficients were calculated using Z statistics after application of Fisher's r to z transform. Other tests, wherever appropriate, are mentioned along with the value. Statistical analyses were performed using SciPy (http://www.scipy.org/) and R (www.r-project.org). Sample sizes in this study are similar to those generally employed in the field and were not pre-determined by a sample size calculation. Data distributions for parametric tests were assumed to be normal, but this was not formally tested.

Tissue processing and immunocytochemistry. Mice were deeply anesthetized with isoflurane/pentobarbital and transcardially perfused with phosphate-buffered saline (PBS) followed by fixative (paraformaldehyde dissolved in PBS, 4%, wt/vol), and brains were extracted and sectioned into 70-µm-thick coronal sections. Sections were washed three times in PBS between each of the following steps. Cell membranes were permeabilized and nonspecific protein binding was blocked by incubation for 1 h in PBS-triton (0.3%) and normal donkey serum (NDS, 10%). Next, sections were incubated for 48 h at 4 °C in a solution of primary antibodies to GFP (used to recognize ChR2-eYFP, 1:500, Aves Labs #GFP-1020, Nacalai Tesque #GF090R/04404-84)[34] and either TH (for the DAT-IRES-Cre brain sections, 1:500, EDM Millipore #AB152, Abcam #ab76442)[35,36] or PV (for the PV-IRES-Cre brain sections, 1:4,000, EDM Millipore #MAB1572), washed and then further incubated in a solution with corresponding secondary antibodies (raised in donkey) conjugated with DyLight488 (1:500, Jackson #703-485-155) or Alexa488 (1:500, Jackson #703-545-155, Invitrogen #A21208) and Cy3 (1:500, Jackson #711-165-152 and #703-165-155; 1:1000, Jackson #715-165-150). Both antibody solutions were diluted in PBS-triton (0.3%) and NDS (1%). Finally, sections were counterstained with DAPI (diluted 1:10,000) for 20 min and mounted on glass slides using VectaShield (Vector Laboratories).

Microscopic analyses and three-dimensional reconstruction. The distribution of transfected axons across brain areas was consistent with the known distribution of dopaminergic fibers[37]. Specificity of virus transfection was quantified from both hemispheres of four bilaterally injected brains. Three consecutive sections centered on the injection coordinate (bregma –3.25) were selected[38]. An exhaustive tiled grid of 20-µm-thick (0.8-µm step) z stacks to span the VTA was acquired from the top of each section using an epifluorescence microscope (Imager.M2 with filter set 38 and a Plan-Neofluar 40×/1.3 objective, Zeiss). Only grid tiles which were deemed to be within the VTA regions (A10 cell groups)[39] were included in the counting. Greater than 900 cells were counted per brain. Three-dimensional reconstruction of transfected dCA1 axons was completed using the same microscope and Neurolucida software (MBF Bioscience). Published images were acquired using a confocal microscope (Imager.Z1 with LSM 710 scan head and Plan-Neofluar 5×/0.16, Plan-Apochromat 40×/1.3, 63×/1.4 or 100×/1.46 objective, Zeiss) in sequential scanning mode with the following excitation laser and emission filter wavelengths. DAPI: 405 nm, 409–499 nm; eYFP/DyLight488: 488 nm, 493–571 nm; Cy3: 543 nm, 566–729 nm. Acquisition and analysis were completed using ZEN 2008, v5.0 (Zeiss) and ImageJ (http://rsb.info.nih.gov/) software. Z stacks were flattened using maximum intensity projection.

A **Supplementary Methods Checklist** is available.

21. Bäckman, C.M. *et al. Genesis* **44**, 383–390 (2006).
22. Cetin, A., Komai, S., Eliava, M., Seeburg, P.H. & Osten, P. *Nat. Protoc.* **1**, 3166–3173 (2006).
23. Tolman, E.C. *Psychol. Rev.* **55**, 189–208 (1948).
24. Csicsvari, J., Hirase, H., Czurkó, A., Mamiya, A. & Buzsáki, G. *J. Neurosci.* **19**, 274–287 (1999).
25. Harris, K.D., Henze, D.A., Csicsvari, J., Hirase, H. & Buzsáki, G. *J. Neurophysiol.* **84**, 401–414 (2000).
26. Harris, K.D., Hirase, H., Leinekugel, X., Henze, D.A. & Buzsáki, G. *Neuron* **32**, 141–149 (2001).
27. Thomson, D.J. *Proc. IEEE* **70**, 1055–1096 (1982).
28. Mitra, P.P. & Pesaran, B. *Biophys. J.* **76**, 691–708 (1999).
29. Grace, A.A. & Bunney, B. *J. Neurosci.* **4**, 2877–2890 (1984).
30. Ungless, M.A. & Grace, A.A. *Trends Neurosci.* **35**, 422–430 (2012).
31. Muller, R.U. & Kubie, J.L. *J. Neurosci.* **9**, 4101–4110 (1989).
32. Skaggs, W.E., McNaughton, B.L., Wilson, M.A. & Barnes, C.A. *Hippocampus* **6**, 149–172 (1996).
33. Zar, J.H. *Biostatistical Analysis* (Prentice Hall, 1999).
34. Tomiyoshi, G., Nakanishi, A., Takenaka, K., Yoshida, K. & Miki, Y. *Cancer Sci.* **99**, 747–754 (2008).
35. Yamamoto, K., Ruuskanen, J.O., Wullimann, M.F. & Vernier, P. *Mol. Cell. Neurosci.* **43**, 394–402 (2010).
36. Samaco, R.C. *et al. Proc. Natl. Acad. Sci. USA* **106**, 21966–21971 (2009).
37. Björklund, A. & Lindvall, O. in *Handbook of Chemical Neuroanatomy, Volume 2: Classical Transmitters in the CNS, Part I* (eds. Björklund, A. & Hökfelt, T.) 55–122 (Elsevier, 1984).
38. Franklin, K.B.J. & Paxinos, G. *The Mouse Brain in Stereotaxic Coordinates* (Academic Press, 2008).
39. Fu, Y. *et al. Brain Struct. Funct.* **217**, 591–612 (2012).

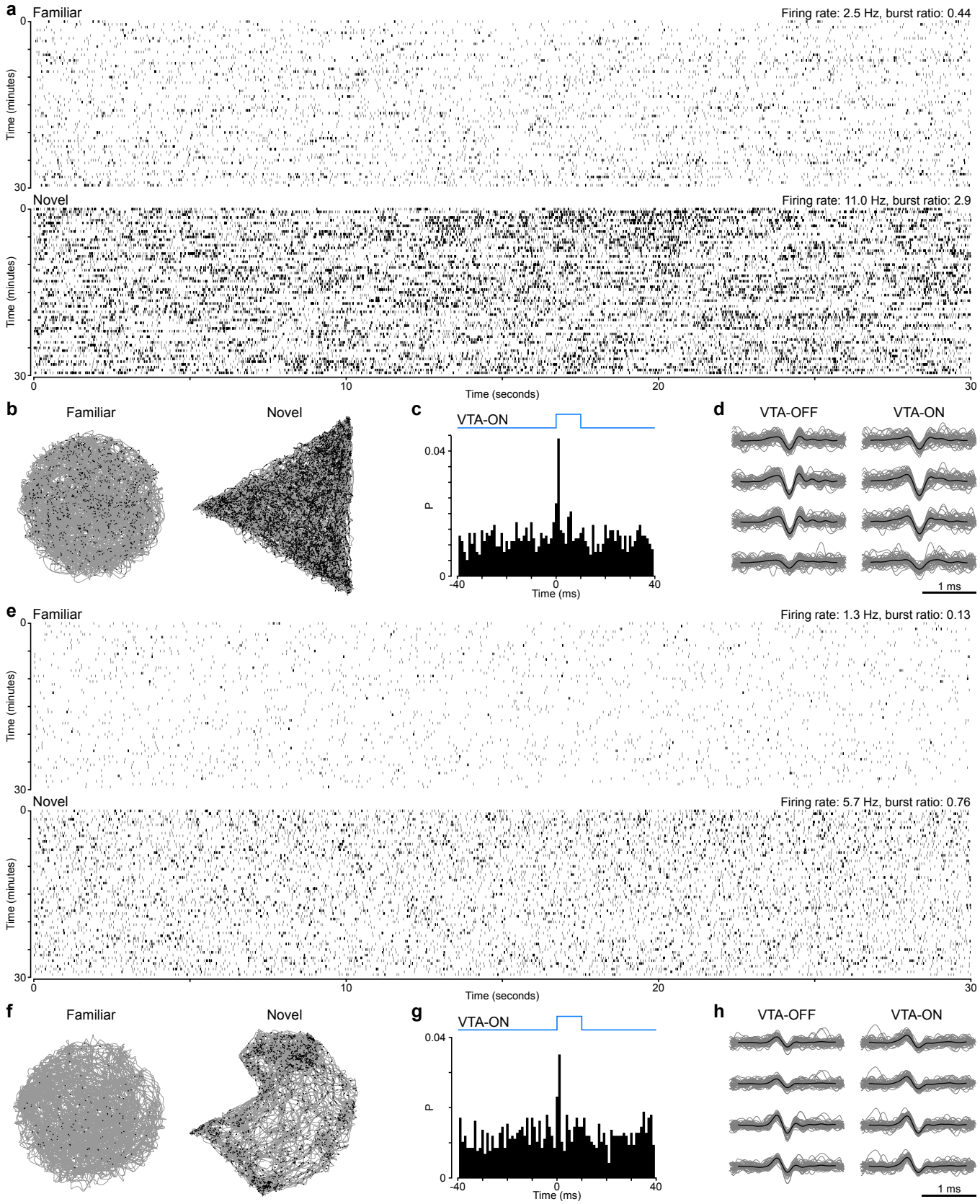

Supplementary Figure 1 Examples of two VTA dopaminergic neurons increasing their firing rate in response to spatial novelty. **(a, e)** Raster plots showing the spike times of the two neurons recorded from a DAT^{VTA}::ChR2-eYFP mouse implanted with tetrodes and an optic fiber in the VTA. The mouse explored a familiar and a novel open field for 30 minutes each environment in the absence of photostimulation (VTA-OFF condition). No food reward was provided in these sessions. Ticks represent spike times (30 seconds exploration per row). Note the strong increase in rate during exploration of the novel environment associated with an increased ratio of bursts of action potentials (defined as at least two spikes within 50 ms; see Methods; gray ticks: single spikes; black ticks: burst spikes). **(b, f)** Spatial distribution of the individual burst action potentials (black dots) discharged by neurons in (a) and (e) superimposed on the animal's path (gray traces) during the respective exploration sessions. **(c, g)** Cross-correlograms of the spike trains of these two neurons to laser pulse onsets subsequently recorded in an additional session while 473 nm light pulses (10 ms pulse) were delivered in the VTA (VTA-ON condition). The onset of light pulses was used as a reference to calculate the probability of spike discharge (1 ms bins). Note the presence of a sharp peak at short latency (< 3 ms) that optogenetically identified these neurons as dopaminergic. **(d, h)** Spike waveforms (gray traces) and superimposed mean waveform (black trace) for these two neurons from VTA-OFF exploration (left) and detected within 3 ms of laser pulse onset in subsequent VTA-ON exploration (right). All four channels of the tetrode are shown (one per row). Note that for each neuron the spike waveforms locked to the laser pulses were similar to those from the earlier exploration.

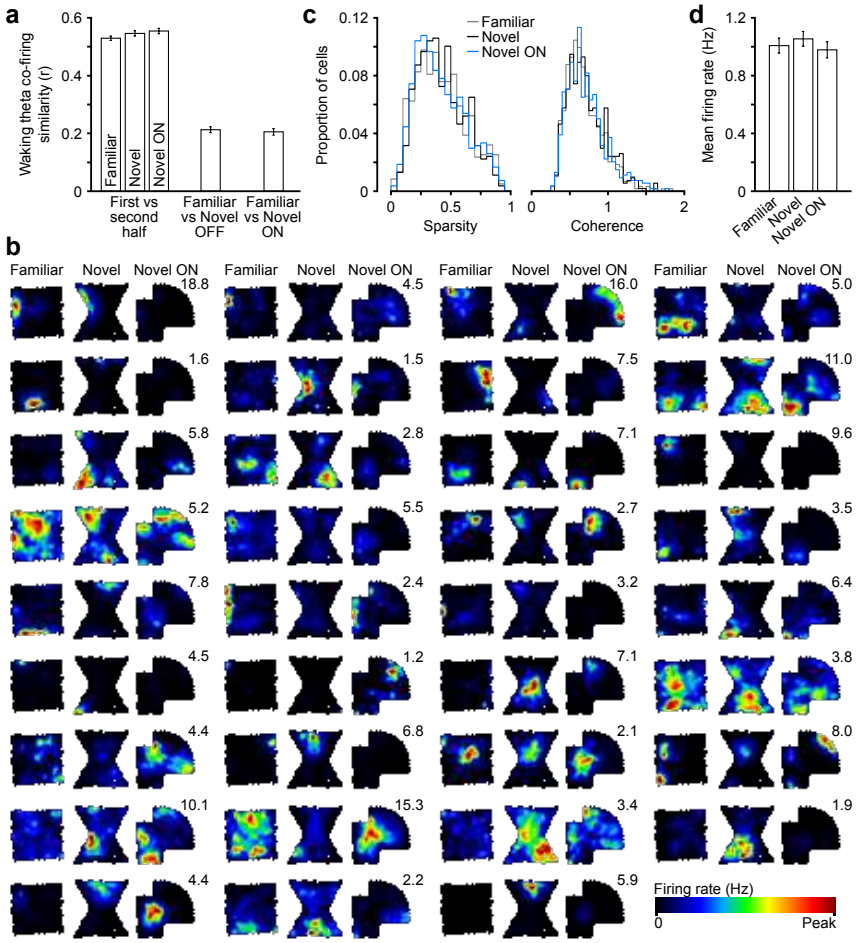

Supplementary Figure 2 Photostimulation of dCA1 dopaminergic axons in DAT^{VTA}::ChR2-eYFP mice did not alter the waking firing activity and cross-environment remapping of hippocampal pyramidal cells. **(a)** Hippocampal representations, as quantified by pyramidal cell co-firing associations (waking theta co-firing similarity), reorganized from the familiar to the novel environments. Waking theta co-firing similarity was measured by correlating the tendency of pyramidal cell pairs to co-fire during cycles of theta-band oscillations in a given exploratory period with such a tendency in another exploratory period. The extent of the novelty-associated hippocampal remapping was unaltered by photostimulation ($Z = 0.46$, $P = 0.65$ for Familiar versus Novel OFF compared to Familiar versus Novel ON). The hippocampal co-firing associations within environments (first versus second half of exploration) were calculated as a reference (all $P < 0.0001$ for each within environment value compared to each across environment value). **(b)** Example of spatial rate maps for a set of dCA1 pyramidal cells from the same recording day followed across different environments and conditions. The peak firing rate (Hz) for each cell is shown. Note the changes in the spatially-selective discharge (i.e., firing field) and/or peak firing rate between environments. **(c)** The distribution of spatial tuning measures was unaltered by photostimulation (sparsity: $P = 0.15$, coherence: $P = 0.80$, Kolmogorov-Smirnov test, Novel OFF versus Novel ON). **(d)** The mean firing rate of dCA1 pyramidal cells was similar across conditions ($F_{2, 1666} = 0.48$, $P = 0.62$, ANOVA).

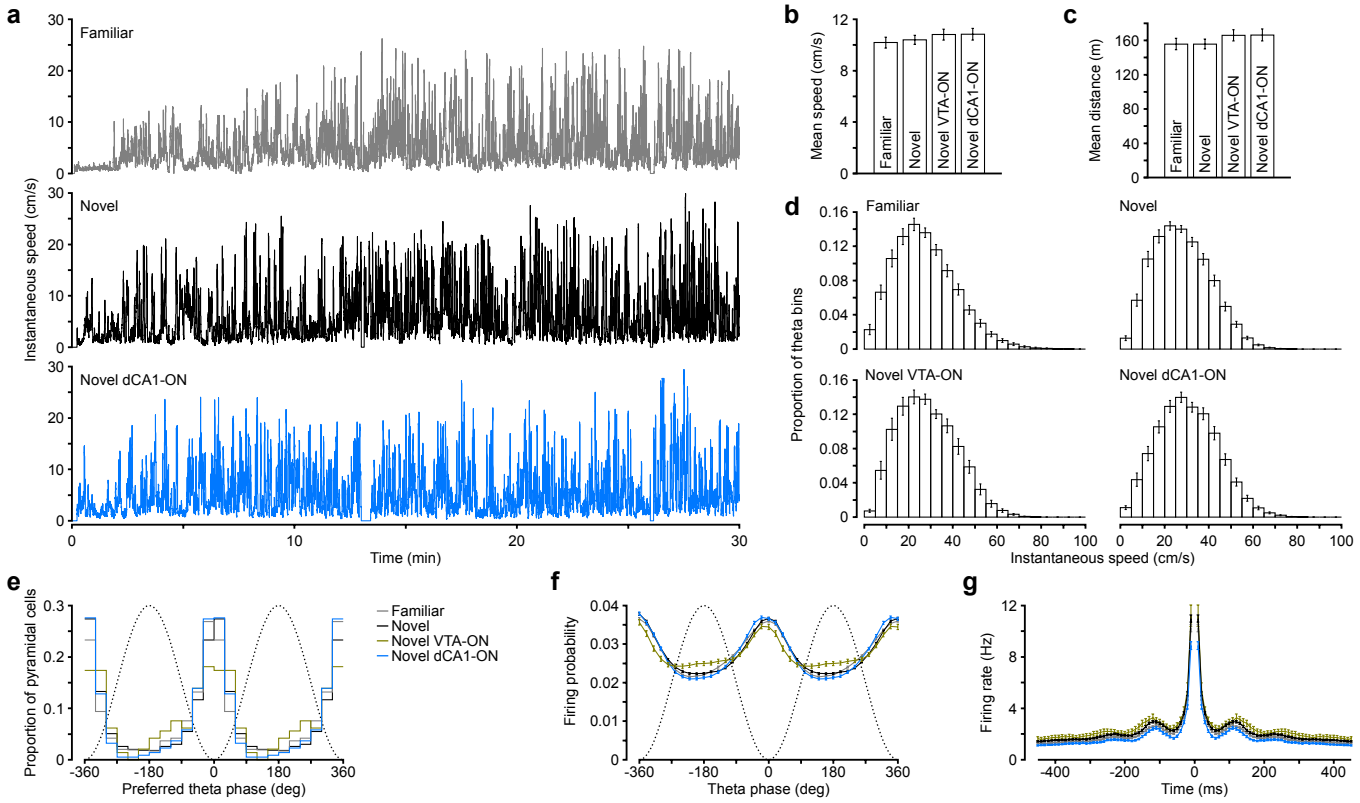

Supplementary Figure 3 Exploratory behavior in the open field environments and pyramidal cell population activity in the theta bins used to calculate waking co-firing. **(a)** Example instantaneous speed plots (820 ms bins) of a DAT^{VTA}::ChR2-eYFP mouse implanted with tetrodes and optic fiber in the dCA1 showing similar movement speed across exploration in the familiar open field and two novel open fields (without photostimulation and with dCA1-ON photostimulation). **(b,c)** The mean speed and mean distance traveled across animals during exploration in the Familiar, Novel and Novel VTA/dCA1-ON conditions were not different (means ± s.e.m.; speed: $F_{3, 143} = 0.44$, $P = 0.72$; distance: $F_{3, 143} = 0.58$, $P = 0.62$; ANOVA). **(d)** Distribution of the instantaneous speed (means ± s.e.m.) in the theta bins used to measure pyramidal cell co-firing in the Familiar, Novel and Novel VTA/dCA1-ON conditions. The distributions are similar and show that theta/waking cofiring measure was confined to epochs of active exploration. **(e)** Distributions of the preferred theta phase for dCA1 pyramidal cells. **(f)** Average firing probability theta-phase histograms of dCA1 pyramidal cells (means ± s.e.m.). Dashed lines represent ideal theta waves. **(g)** Average autocorrelation histograms of dCA1 pyramidal cells (10 ms bins). These data indicate that the waking firing-phase coupling of pyramidal cells to theta oscillations was similar across conditions and that the theta co-firing measure was confined to epochs of theta-paced hippocampal activity.

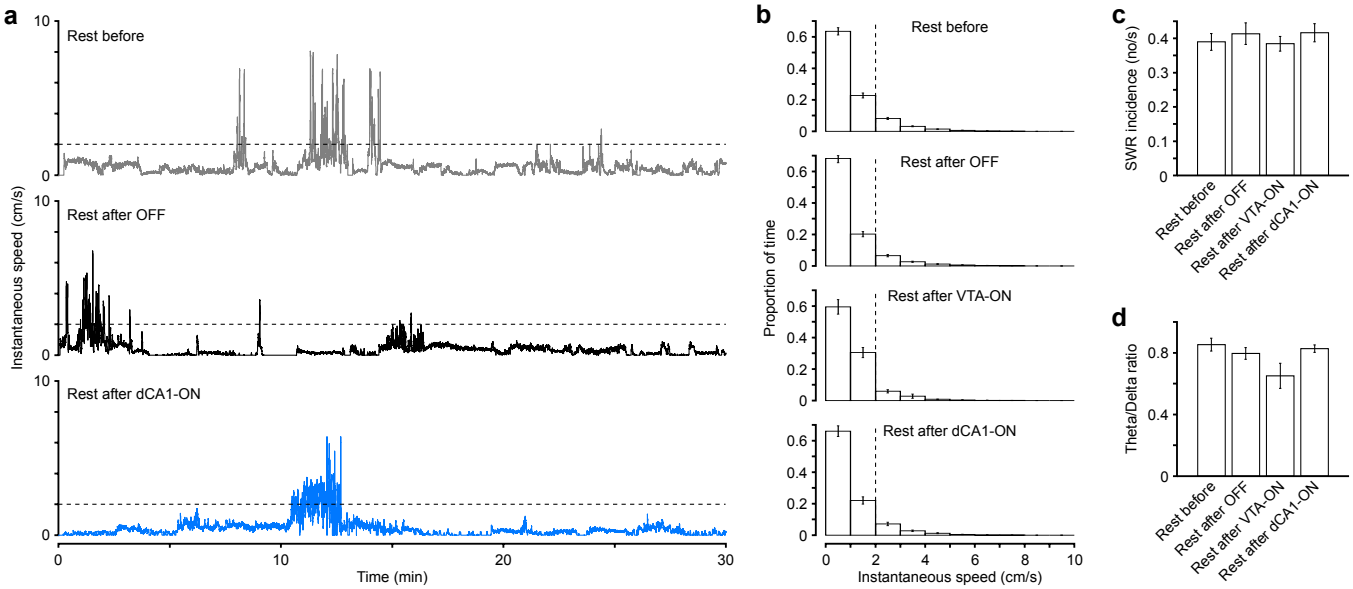

Supplementary Figure 4 Behavioral and electrophysiological estimates of arousal states were similar in the rest sessions preceding and following exploration. **(a)** Example instantaneous speed plots (820 ms bins) of a DAT^{VTA}::ChR2-eYFP mouse implanted with tetrodes and optic fiber in the dCA1 during rest in the sleep box before open field explorations, after exploration of a novel open field and after exploration of a novel open field with dCA1-ON photostimulation. Note that the animal spent most of its time immobile (instantaneous speed < 2cm/s; dashed line) in all conditions. **(b)** The distributions of the instantaneous speed (means ± s.e.m.) across animals. The proportion of time spent immobile (left of the 2 cm/s dashed line) was similar during the sleep/immobility rest sessions before exploration and after exploration across conditions. **(c)** The number of SWRs per second was similar in rest before exploration and after exploration across conditions (means ± s.e.m.; $F_{3, 143}$ = 0.24, P = 0.86, ANOVA). **(d)** The theta/delta band power ratio (means ± s.e.m.; $F_{3, 143}$ = 2.10, P = 0.10, ANOVA; see Methods) was not significantly different in rest before exploration and after exploration across conditions. Note that the slight non-significant decrease of theta/delta ratio during rest after the VTA-ON condition was not observed in the dCA1-ON condition and thus cannot account for the photostimulation-enhanced reactivation.

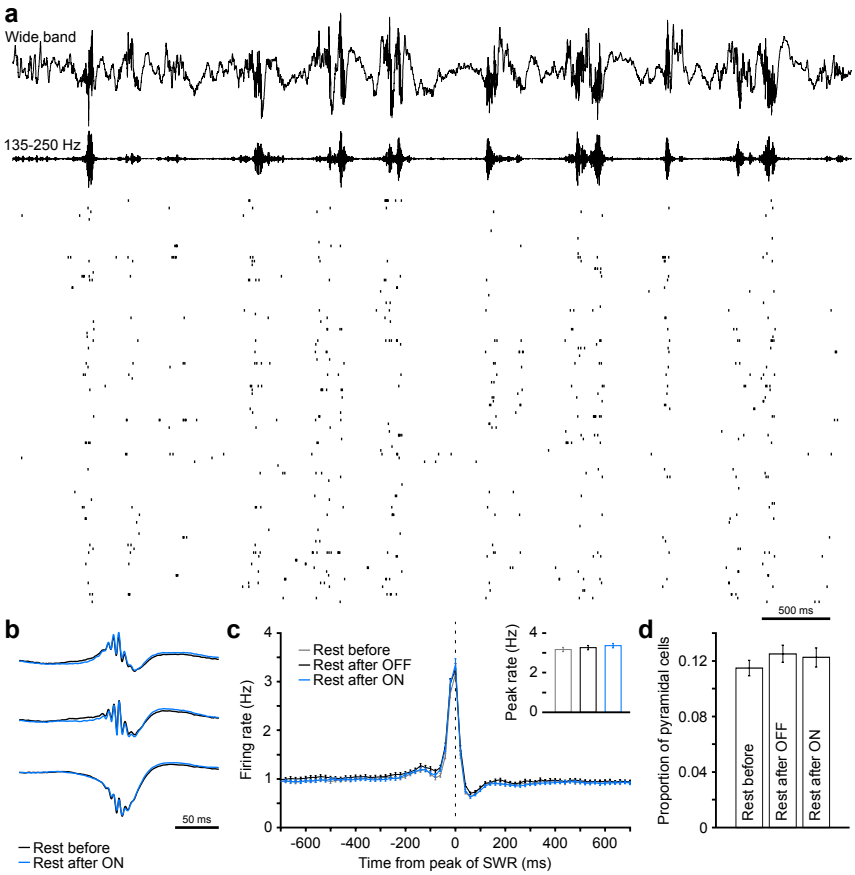

Supplementary Figure 5 Sharp-wave/ripple firing responses of dCA1 pyramidal cells during rest. **(a)** Top trace, wide band signal. Bottom trace, 135–250 Hz band pass filtered signal highlighting ripple frequency events. Raster plots, spike times of simultaneously recorded dCA1 pyramidal cells (one cell per row). Note the firing synchrony of pyramidal cells during ripple events. **(b)** Mean SWR-triggered waveforms from three separate tetrodes in a DAT^{VTA}::ChR2-eYFP mouse during rest before and after dCA1-ON photostimulation. Traces obtained from the same tetrode (one channel displayed) are superimposed. **(c)** SWR-triggered firing rate histograms (means ± s.e.m.) of dCA1 pyramidal cells from all DAT^{VTA}::ChR2-eYFP mice during rest sessions preceding and following exploratory sessions with or without photostimulation. SWR firing rate histograms were calculated using 20 ms bins in reference to the SWR peak (i.e., peak of ripple-band power). The mean peak SWR firing rate was unaltered by photostimulation ($F_{2, 2892} = 0.86$, $P = 0.42$, ANOVA). **(d)** The proportion of SWR-active pyramidal cells (i.e., for each SWR the proportion of cells discharging at least one spike) in rest sessions preceding and following exploratory sessions with or without photostimulation was similar (means ± s.e.m.; $F_{2, 129} = 0.78$, $P = 0.46$, ANOVA).

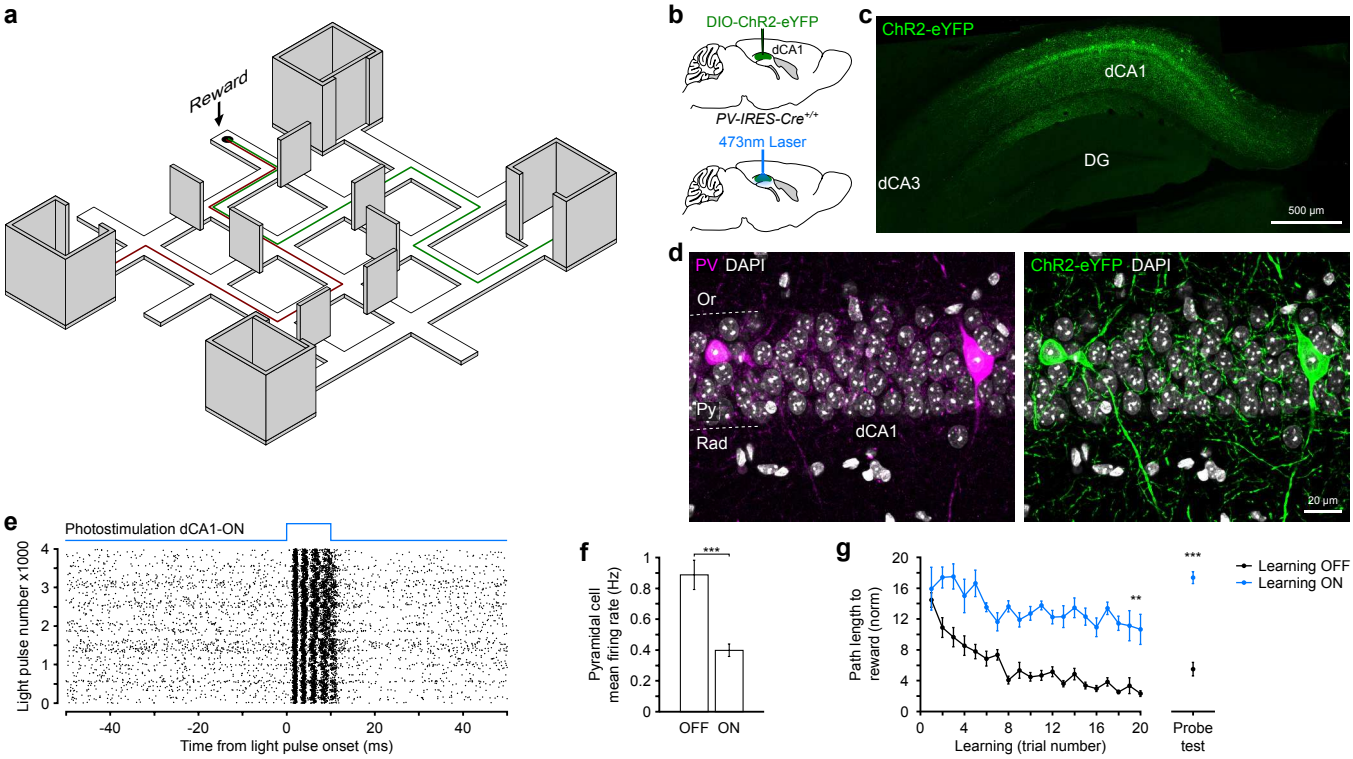

Supplementary Figure 6 Spatial learning on the crossword maze requires a functional hippocampal network. **(a)** Isometric projection of the crossword maze showing an example configuration of barriers and reward location. On any given recording day only two of the start boxes were used. The shortest paths from the in use start boxes to the reward location are shown in red and green. **(b)** In order to disrupt locally the activity of dCA1 hippocampal pyramidal cells, the Cre-inducible viral construct coding for Channelrhodopsin-2 (ChR2-eYFP) was injected into the dCA1 of Parvalbumin PV-IRES-Cre$^{+/+}$ mice. To control and monitor dCA1 pyramidal cell activity these PV^{dCA1}::ChR2-eYFP mice were implanted in dCA1 for combined in vivo multichannel recordings with photostimulation. **(c)** Low magnification image showing the expression of ChR2-eYFP targeted to the dCA1 of a PV^{dCA1}::ChR2-eYFP mouse. **(d)** High magnification confocal image of the dCA1 showing expression of ChR2-eYFP in PV-expressing interneurons (flattened 5 µm z-stack). Cell nuclei stained with DAPI. **(e)** Raster plot showing the spike times of one dCA1 interneuron recorded in a PV^{dCA1}::ChR2-eYFP mouse in relation to the onset of 10 ms light pulses in the dCA1-ON condition. Note the increased spiking activity with short latency (< 3 ms) induced by the laser and confined to the duration of the stimulation pulse. **(f)** Photostimulation of dCA1 (dCA1-ON) in these PV^{dCA1}::ChR2-eYFP mice led to a decrease in firing rate of dCA1 pyramidal cells (n = 224; t_{222} = 5.01, P = 1.1x10^{-6}, t-test). **(g)** Left, learning performance, as measured by distance traveled to reward, was impaired in days when the PV^{dCA1}::ChR2-eYFP mice received photostimulation (see Methods; group x trial interaction, $F_{19, 354}$ = 2.08, P = 0.0054, ANOVA). Right, photostimulation applied during learning was associated with subsequent degraded performance during the probe test (t_{19} = 9.81, P = 7.1x10^{-9}, t-test).

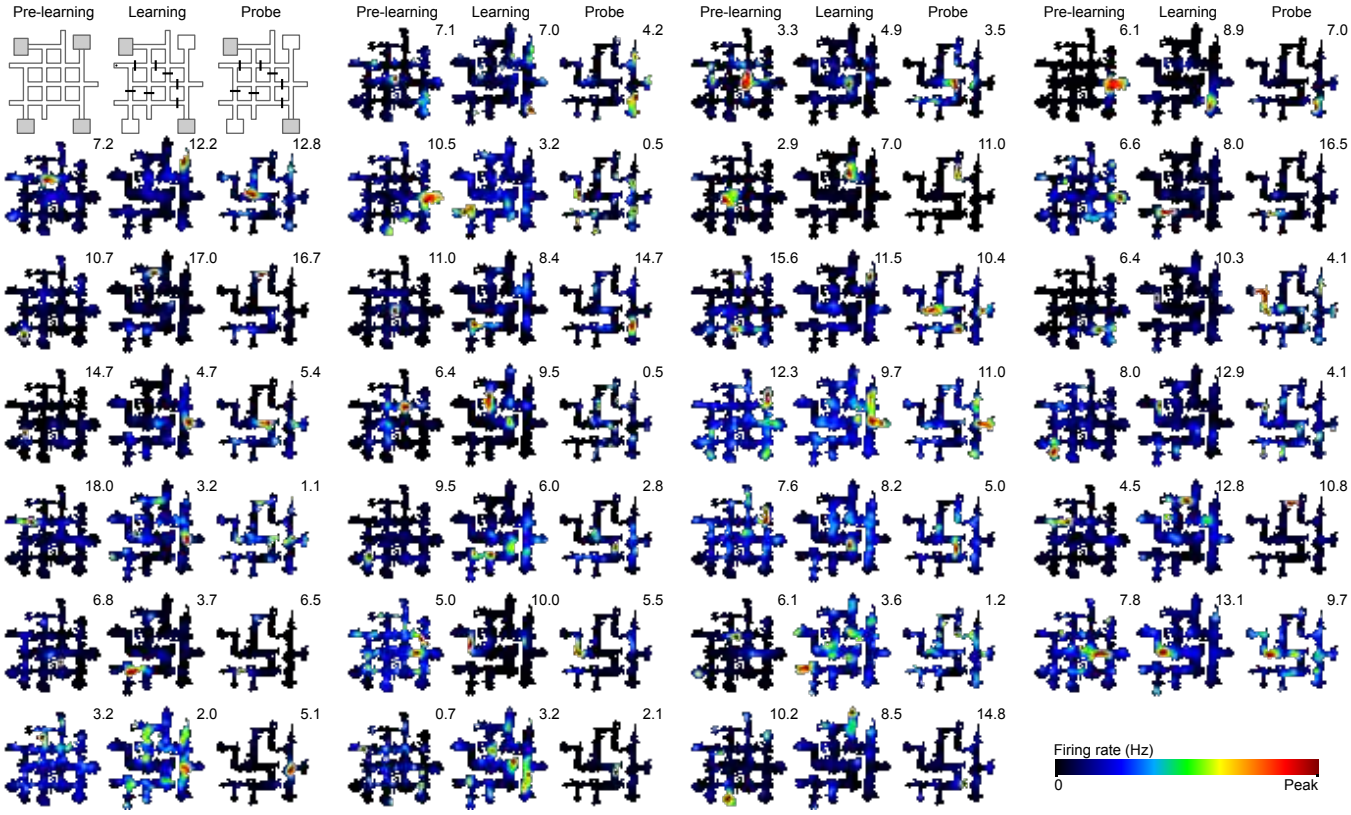

Supplementary Figure 7 Examples of dCA1 hippocampal maps recorded from a DAT^{VTA}::ChR2-eYFP mouse on the crossword maze. Shown are the spatial rate maps for a set of dCA1 pyramidal cells from the same recording day followed across the Pre-learning, Learning and Probe stages. The peak firing rate (Hz) for each map is shown. The maze configuration for that day is depicted in the top left. Note that most cells established new firing fields in learning compared to pre-learning and many but not all reinstated the newly-established maps during the probe test.

Supplementary Table 1 Recording sessions and cell counts for DAT-IRES-Cre$^{+/-}$ mice

Number of recording sessions - Number of pyramidal cells - Number of pyramidal cell pairs

	Familiar	Novel	Novel VTA-ON burst	Novel dCA1-ON burst	Novel dCA1-ON burst eYFP ctrl.	Novel dCA1-ON burst SCH23390	Novel dCA1-ON tonic	Crossword dCA1-OFF	Crossword dCA1-ON
Per individual animal	6 - 88 - 668	6 - 89 - 684		4 - 53 - 340			2 - 34 - 297		
	6 - 132 - 1457	6 - 130 - 1404		4 - 84 - 885			2 - 47 - 535		
	5 - 55 - 290	6 - 64 - 346		8 - 79 - 412			4 - 42 - 252		
	3 - 103 - 1731	3 - 113 - 2082		7 - 212 - 3324			5 - 148 - 2329		
	3 - 16 - 39	3 - 20 - 57	4 - 23 - 56						
	10 - 109 - 580	10 - 125 - 850	9 - 103 - 664						
	7 - 47 - 175	4 - 22 - 52		4 - 22 - 52		3 - 26 - 117			
	4 - 168 - 3973	3 - 120 - 2932		2 - 88 - 2036		5 - 205 - 4755			
	4 - 32 - 131	6 - 36 - 115			7 - 42 - 137				
	5 - 258 - 8706	5 - 266 - 9262			5 - 265 - 9294				
								3 - 16 - 52	3 - 53 - 598
								3 - 33 - 361	3 - 89 - 1398
								1 - 4 - 6	3 - 18 - 108
								5 - 191 - 5642	4 - 156 - 3907
Total	53 - 1008 - 17750	52 - 985 - 17784	13 - 126 - 720	29 - 538 - 7049	12 - 307 - 9431	8 - 231 - 4872	13 - 271 - 3413	12 - 244 - 6061	13 - 316 - 6011

Supplementary Table 2 Baseline correlations (Rest before) versus reactivation strength (Rest after)

	Rest before correlation coefficient*	Rest after correlation coefficient*	Rest before vs Rest after Z-value	P-value
Familiar	0.066 ± 0.007	0.126 ± 0.007	-5.7	1.0E-08
Novel	0.059 ± 0.007	0.175 ± 0.007	-11.1	9.0E-29
Novel VTA-ON burst	0.032 ± 0.037	0.267 ± 0.036	-4.6	4.8E-06
Novel dCA1-ON burst	0.068 ± 0.012	0.263 ± 0.011	-11.9	6.9E-33
Novel dCA1-ON burst eYFP ctrl.	0.052 ± 0.010	0.171 ± 0.010	-8.2	1.6E-16
Novel dCA1-ON burst SCH23390	0.042 ± 0.014	0.143 ± 0.014	-5.1	3.9E-07
Novel dCA1-ON tonic	0.036 ± 0.017	0.210 ± 0.017	-7.3	2.3E-13
Crossword Pre-learning	0.051 ± 0.010	0.106 ± 0.010	-4.1	4.6E-05
Crossword Learning dCA1-OFF	0.054 ± 0.013	0.173 ± 0.013	-6.6	3.6E-11
Crossword Learning dCA1-ON	0.046 ± 0.013	0.228 ± 0.013	-10.2	1.7E-24

*Pearson correlation coefficient ± the standard error of the correlation coefficient

Supplementary Table 3 Comparison of reactivation strength (Rest after) across conditions

Z values

Familiar	4.79	3.87	10.12	3.61	1.10	4.66	-1.61	3.25	7.10
1.7E-06	Novel	2.53	6.52	-0.38	-2.04	1.94	-5.78	-0.17	3.69
0.00011	0.011	Novel VTA-ON burst	-0.12	-2.62	-3.24	-1.47	-4.33	-2.51	-1.05
4.3E-24	7.2E-11	0.9	Novel dCA1-ON burst	-6.13	-6.69	-2.66	-10.59	-5.38	-2.09
0.00031	0.7	0.0088	8.6E-10	Novel dCA1-ON burst eYFP ctrl.	-1.59	2.06	-4.66	0.14	3.63
0.27	0.042	0.0012	2.2E-11	0.11	Novel dCA1-ON burst SCH23390	3.10	-2.17	1.58	4.57
3.2E-06	0.052	0.14	0.0078	0.04	0.0019	Novel dCA1-ON tonic	-5.43	-1.81	0.88
0.11	7.7E-09	1.5E-05	3.3E-26	3.2E-06	0.03	5.5E-08	Crossword (Cw.) Pre-learning	4.23	7.80
0.0012	0.87	0.012	7.5E-08	0.89	0.11	0.07	2.3E-05	Cw. Learning dCA1-OFF	3.16
1.3E-12	0.00022	0.29	0.037	0.00028	5.0E-06	0.38	6.1E-15	0.0016	Cw. Learning dCA1-ON

P values